THE ASTROPHYSICAL JOURNAL, 430:682–689, 1994 August 1

HIGH RYDBERG STATE CARBON RECOMBINATION LINES TOWARD CASSIOPEIA A: 332 MHz VLA OBSERVATIONS AND COMPARISON WITH H I AND MOLECULAR LINES

K. R. ANANTHARAMAIAH,[1] W. C. ERICKSON,[2] H. E. PAYNE,[3] AND NIMISHA G. KANTHARIA[1,4]
Received 1993 April 30; accepted 1994 January 26

ABSTRACT

We present observations of the C270α carbon recombination line, 21 cm neutral hydrogen line and ^{12}CO ($J = 1 \rightarrow 0$) molecular line toward Cas A. A comparison of the distribution of recombination line optical depths over the face of Cas A with that of H I optical depths and molecular line emission favors the association of C270α regions with H I rather than molecular clouds. The association makes it possible to self-consistently determine several physical parameters of the clouds by combining the recombination line and 21 cm H I measurements.

Subject headings: ISM: abundances — ISM: molecules — radio lines: ISM

1. INTRODUCTION

The line of sight to the strong radio source Cassiopeia A, which intersects the Perseus and the Orion arms, has provided unique results on radio recombination lines from highly excited states of carbon. A number of observations have been made at frequencies ranging from 14.7 MHz (Konovalenko 1990) to 1425 MHz (Sorochenko & Walmsley 1991). This corresponds to principal quantum numbers in the range from $n = 766$ to $n = 166$. The lines from higher quantum numbers ($n > 400$), which appear at frequencies of tens of MHz, are the first radio recombination lines to be observed in absorption. On the other hand, the lines which appear at frequencies above 200 MHz ($n < 330$) are in emission, even though the brightness temperature of the background source Cas A is several million degrees at these frequencies. As discussed by Payne, Anantharamaiah, & Erickson (1989, hereafter PAE89), this is direct evidence for stimulated emission of recombination lines for cold clouds in the Perseus and the Orion arms.

The detected lines have three velocity components. Two of the components are near -37 and -47 km s^{-1}, which correspond to the Perseus arm in this direction, and the other component is near 0 km s^{-1}, corresponding to the Orion arm. The Perseus arm components have been detected at most of the observed frequencies, and the weaker Orion arm component has been detected in only two of the observations (PAE89; Konovalenko 1990). These velocities are similar to what is seen in λ21 cm H I absorption and also in several molecular lines like OH, H_2CO, NH_3, and CO. It now seems well established that the carbon recombination lines come from clouds where gas-phase carbon is more or less completely ionized and hydrogen is mostly neutral, in either atomic or molecular form (Blake, Crutcher, & Watson 1981; Walmsley & Watson 1982; Ershov et al. 1984; PAE89; Konovalenko 1990; Sorochenko & Smirnov 1990). However, it is not yet clear whether the observed lines are associated with neutral hydrogen or molecular gas, both of which are found at similar velocities in this direction. As a consequence, two types of models, referred to as warm gas and cold gas models, have been proposed. In the warm gas models the carbon recombination line region is thought to be associated with the neutral H I clouds where the temperature is in the range 50–100 K. In the cold gas models the temperature of the C II region is in the range 10–20 K, and therefore it is likely to be associated with molecular gas. For the warm gas models, the pressure broadening of the recombination lines observed at the lowest frequencies implies electron densities in the range 0.1–0.06 cm^{-3}, and for the cold gas models the densities are 0.5 to 0.25 cm^{-3}. The observed pressure broadening cannot distinguish between the cold and warm gas models.

The observed intensity of the lines as a function of frequency has also been used to infer the physical condition in the clouds (Ershov et al. 1984, 1987; PAE89; Konovalenko 1990; Sorochenko & Smirnov 1990). This subject is reexamined at length in a second paper (Payne, Anantharamaiah, & Erickson 1994, hereafter PAE94). Modeling the line intensities requires explicit calculation of the level populations in these high Rydberg states for a given combination of temperature, density, and background radiation. In the cold gas models, where $T = 10$–20 K, singly ionized carbon atoms are expected to behave essentially like ionized hydrogen, and therefore hydrogenic computation of the level populations such as those by Shaver (1975) or Salem & Brocklehurst (1979) have been used. It was suggested by Watson, Western, & Christensen (1980) that in the warm gas models it is necessary to include a dielectronic-like recombination process which significantly influences the level population in the high Rydberg states of carbon. This process works only in warm clouds since electrons with energy ~92 K are required to excite the fine structure transition $^2P_{1/2} \rightarrow {}^2P_{3/2}$ in the ground state of singly ionized carbon. Using the calculations of the level populations by Walmsley & Watson (1982), which include the above process, several attempts were made to fit the observed variation of line strength with frequency (Ershov et al. 1984, 1987; PAE89; Konovalenko 1990; Sorochenko & Smirnov 1990). Although both the warm and the cold gas models fit some aspects of the observed data, neither model provided a completely satisfactory fit over the entire observed frequency range (see PAE89). When the observations reported here were made,

[1] Raman Research Institute, Bangalore 560 080, India.
[2] Physics Department, University of Tasmania, Box 252C, GPO Hobart, Tasmania 7001, Australia.
[3] Space Telescope Science Institute, 3700 San Martin Drive, Baltimore, MD 21218.
[4] Joint Astronomy Program, Physics Department, Indian Institute of Science, Bangalore 560 012, India.

it was not at all clear whether the observed C II region is associated with neutral H I or molecular clouds in the direction of Cas A. In a second paper (PAE94) we show that these analyses were hampered by a systematic error in the observations at the lowest frequencies and an unphysical boundary condition imposed on the level population calculation. After correcting for these problems, we find that the observations make sense only if the recombination lines originate in the atomic gas. So it remains critically important to find other evidence for deciding between atomic and molecular clouds as the source of the recombination lines.

Fortunately, there is an additional datum which can be used to choose between the atomic and molecular gas models: the spatial distribution of the recombination lines. The H I clouds observed at $\lambda 21$ cm (e.g., Schwarz et al. 1986; Bieging, Goss, & Wilcots 1991) and molecular clouds observed in H_2CO, OH, NH_3, and CO (e.g., de Jager et al. 1979; Batrla, Walmsley, & Wilson 1984; Goss, Kalberla, & Dickel 1984; Troland, Crutcher, & Heiles 1985) have different distributions across the face of Cas A. Since PAE89 have shown that the carbon recombination lines are detectable at 325 MHz, it is possible to use the Very Large Array (VLA) to determine the distribution of these lines over the face of Cas A and compare that with the available molecular and H I distributions.

In this paper we present such a comparison. We have observed the distribution of the C270α (332.42 MHz) recombination line across the face of Cas A using the VLA. We obtain the H I distribution from Westerbork Synthesis Telescope data of Kalberla, Schwarz, & Goss (1994). The distribution of molecular gas was determined by mapping the ^{12}CO ($J = 1 \rightarrow 0$, 115.27 GHz) line emission over the face of Cas A using the 10.4 m telescope at a Raman Research Institute, Bangalore. The observations are described in § 2. The distribution of C270α is compared with that of H I and molecular gas in § 3 and the implications are discussed in § 4.

2. OBSERVATIONS

2.1. *C270α Recombination Line Using the VLA*

Observations of the C270α line were made in four different sessions during 1987–1988 using the VLA in its C- and D-configurations. At the time of these observations only 15–18 of the 27 VLA antennas were equipped with 332 MHz feeds and receivers. When pointing to Cas A, the system temperature of the individual antennas was about 550 K. Off-source system temperature was typically 125 K. The maximum antenna separations for these configurations are 3 km and 1 km, respectively. The observations were made using 64 spectral channels centered at an LSR velocity of -37 km s^{-1}. The spectral resolution was 1.38 km s^{-1}. Interspersed observations of 3C 48 were used to calibrate the instrumental amplitude, phase, and frequency response. The flux density of 3C 48 was assumed to be 44.31 Jy at the observing frequency.

The calibrated data from all the four sessions were combined to make a single spectral line database of 63 channels and one continuum database formed by averaging the central three-quarters of the observed band. The net effective integration time for the edited database was about 13 hr. Continuum emission in the line channels was removed in two stages. First, a continuum image was made and deconvolved using "CLEAN." The "clean components," with a total flux density of 6000 Jy, were Fourier-transformed and subtracted from the visibility data in each of the line channels. Using the continuum-subtracted line data, channel images were constructed using natural weighting of the visibility data. Residual continuum in the line images was then removed by subtracting an average image of the channels where no spectral emission was expected. In the final 63 line images, line emission was found near velocities of -1.2 km s^{-1}, corresponding to the Orion arm, and -37 and -47 km s^{-1}, corresponding to the Perseus arm. The rms noise in the line images is $\sim$0.2 Jy beam^{-1}. The line images where emission was seen were deconvolved using "CLEAN." The half-power width of the naturally weighted beam is 2.″7 × 2.″4 (P.A. = 49.°6). An optical depth spectrum was constructed by integrating the flux density in each of the line images over the same area where continuum emission is seen, and dividing by the total continuum. This spectrum is shown in Figure 1. (The line is in emission, as shown, which means that the optical depths are negative.) The features mentioned above can be identified in this spectrum. The line parameters of the three features are given in Table 1.

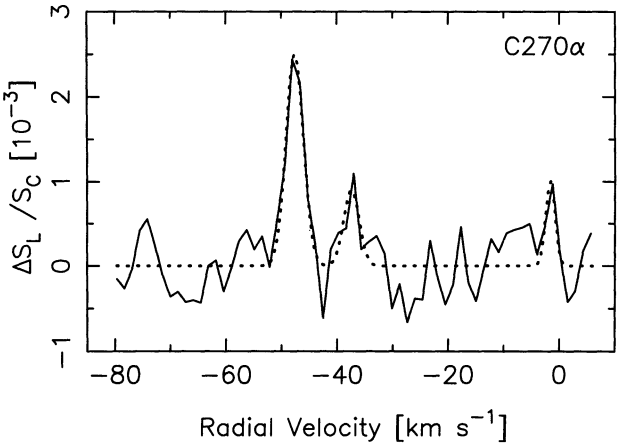

FIG. 1.—The average C270α spectrum of Cas A, obtained by integrating the line flux ΔS_L over the face of Cas A and dividing by the total continuum flux S_C. The dotted line shows the three Gaussian components fitted to the spectrum.

The final continuum image and spectral line images corresponding to the three features (each averaged over a velocity range as indicated) are shown in Figure 2. The observed peak continuum and line brightnesses are 2363.6 Jy beam^{-1} and 6.34 Jy beam^{-1}, respectively. The integrated continuum flux density of Cas A is 6691 Jy, which is about 5% higher than the value predicted by Baars et al. (1977). As discussed by Bieging et al. (1991), this excess flux is an artifact of the errors in the correction of the digitally measured visibility function. Such an error occurs in the VLA correlator system for strong sources like Cas A. This error, which is at the most 5% in this case, is likely to be even smaller for the optical depth maps, which are

TABLE 1

LINE PARAMETERS OF THE INTEGRATED PROFILE

Feature	V_{LSR} (km s^{-1})	τ_L ($\times 10^3$)	ΔV_{FWHM} (km s^{-1})
Perseus arm	-47.6 ± 0.1	2.5 ± 0.2	3.7 ± 0.3
	-37.4 ± 0.4	0.9 ± 0.2	3.3 ± 0.8
Orion arm	-1.6 ± 0.2	1.0 ± 0.3	2.0 ± 0.6

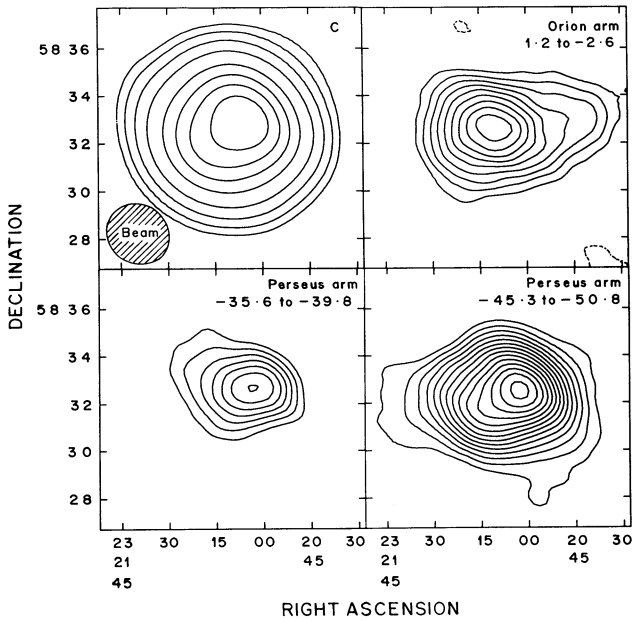

FIG. 2.—Continuum and C270α line images of Cas A obtained using combined C- and D-configuration data, with natural weighting. The beam size is 2.″7 × 2.″4 with P.A. = 49.°6. The image at the top left corner marked C is the continuum image. The contour levels for this image are 50, 100, 200, and 400 to 2400 in steps of 400 Jy beam.$^{-1}$. The line images correspond to the three features near 0, −37, and −47 km s^{-1} seen in Fig. 1. The line images are averaged over the velocity range indicated in each frame. The lowest contour level for the line images is 0.4 Jy beam^{-1} and the contour interval is 0.2 Jy beam.$^{-1}$

constructed by forming the ratio of line and continuum flux densities. As can be seen in Figure 2, the peaks of the line emission for the Perseus arm features are displaced from the continuum peak. The feature near −47 km s^{-1} is seen over almost the entire face of Cas A, whereas the −37 km s^{-1} feature is concentrated in the central region. The Orion arm feature appears to have two distinct spatially separated components.

The distribution of the optical depth of the C270α line, across the face of Cas A, was obtained by dividing the individual line images by the continuum image. For the small opacities expected in the line, the optical depths can be approximated by $\tau = -\Delta S_L/S_C$, where ΔS_L is the line intensity after subtracting the continuum and S_C is the continuum intensity at each pixel. The regions of the image with continuum flux density less than 60 Jy beam^{-1} (5 σ level) are blanked in the optical depth maps. The resulting opacity maps, along with the continuum, are shown in Figure 3. It should be noted that the apparent increase in the optical depths toward the edge of the source is an artifact of the division by the continuum, which naturally has low values at the edges. The noise fluctuations are amplified by more than a factor of 10 relative to the center. More significance should therefore be given to the distribution observed in the central regions of the source.

Even with the coarse angular resolution (2.″7 × 2.″4), some structure can be seen in the distribution of C270α optical depths. The strong Perseus arm features at −46.6 and −48 km s^{-1} show gradients in the opacity running almost diagonally from northeast to southwest, and there appears to be a clump of ionized C II near the southwest corner. At velocities of −49.4 and −50.8 km s^{-1} the gradient runs from east to west, with a concentration in the eastern half. The other Perseus arm feature, centered at −37 km s^{-1}, also has structure with a concentration towards the western half of the source. The Orion arm feature at −1.2 km s^{-1} shows increasing opacity toward the western edge of Cas A.

2.2. H I *Data*

Aperture synthesis observations of the distribution of H I opacity in the Perseus arm features at −37 and −48 km s^{-1} with an angular resolution of 1′ have been reported by Schwarz et al. (1986) and with much higher angular resolution (7″) by Bieging et al. (1991). In order to make a proper comparison with the present C270α data, we have obtained unpublished Westerbork Synthesis Telescope data from Kalberla et al. (1994) and smoothed them in both velocity and space to match our resolution. The original data have an angular resolution of 28.″6 × 23.″9 and a velocity resolution of 0.515 km s^{-1}. The optical depth maps were computed using a cutoff of 30 Jy in the convolved continuum distribution. The results are shown in Figure 4. There are small differences between the central velocities of the opacity maps shown in Figures 3 and 4. The velocity resolution of the H I opacity maps is 1.55 km s^{-1} and that of the C270α maps is 1.38 km s^{-1}. The H I optical depth map at −48.2 km s^{-1} is saturated over a large region.

2.3. ^{12}CO ($J = 1 \rightarrow 0$) *Observations Using the RRI 10.4* m *Telescope*

The ^{12}CO line at 115.27 GHz was mapped in two sessions in 1991 and 1993 over a 13′ × 13′ region centered on Cas A using the 10.4 m telescope at the Raman Research Institute, Bangalore. The angular resolution is ∼1′ and the grid spacing was 0.′5 in R.A. and 1′ in Decl. As the observations were made during day time, the pointing accuracy was ∼10″. The double sideband system temperature was between 1200 K to 1800 K depending on atmospheric conditions. A chopper wheel was used to calibrate the antenna temperature (T_A^*) corrected for atmospheric absorption. The data were recorded in frequency-switched mode in a 256 channel filter bank with a resolution of 250 kHz (or 0.65 km s^{-1}). Individual spectra were smoothed to match the resolution (1.3 km s^{-1}) of the C270α observations. The rms noise in the spectra was typically 0.3 K. ^{12}CO emission over the face of Cas A at the Orion and Perseus arm velocities (where C270α line was observed) is shown in Figure 5. The distribution of ^{12}CO emission, seen in Figure 5, is consistent with earlier observations by Troland et al. (1985) with similar resolution.

3. COMPARISON OF C270α, H I, AND MOLECULAR LINES

A comparison of Figures 3 and 4 shows that the C270α and H I opacity distributions have very similar trends at a number of velocities. However, they are not identical. The H I opacity maps have much higher signal-to-noise ratio (S/N) and therefore they look much smoother than the C270α opacities. The similarity between the two is close at almost all the Perseus arm velocities. The similarity is striking at velocities of −37, −38.5, −46.7, −49.4, and −50.8 km s^{-1}. The direction of the gradient in optical depths and the position of the peaks in the two sets of maps are very similar at these velocities. The distributions are not so similar at the Orion arm velocities of −1.2 and −2.6 km s^{-1}. Unfortunately, at −48 km s^{-1}, where the C270α has the highest S/R, the H I opacity map is saturated, and therefore a comparison is not very meaningful.

On the other hand, a comparison between Figures 3 and 5 shows that there is very little similarity between the C270α

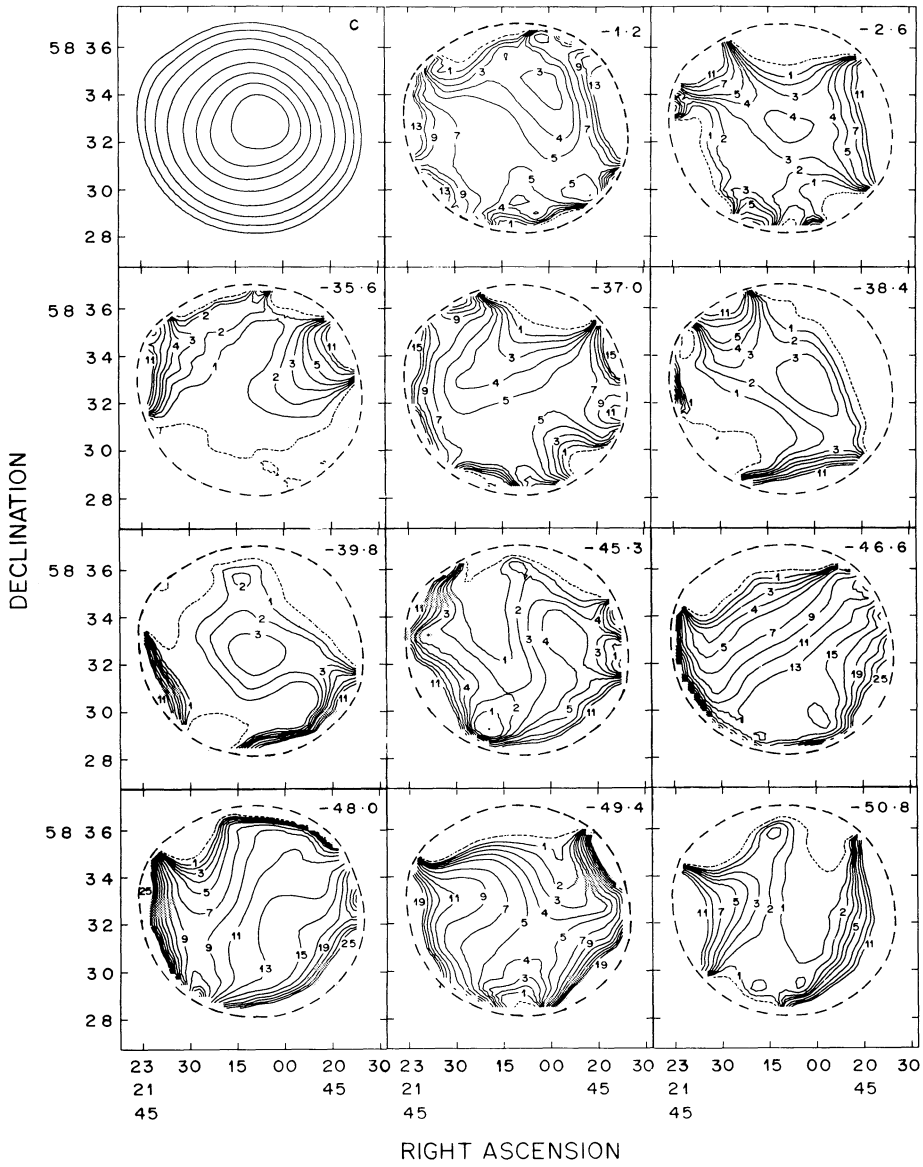

FIG. 3.—The distribution of C270α optical depths at velocities where line emission was seen. The velocities are indicated (in km s^{-1}) at the top right corner of each frame. The beam size is 2.″7 × 2.″4 with P.A. = 49.°6, and the velocity resolution is 1.38 km s^{-1}. The image at the top left corner is the continuum distribution, which has the same contour levels as in Fig. 2. Contour levels for the optical depth images are: −1, 1 to 5 in steps of 1 and 7 to 25 in steps of 2 units where 1 unit = 2×10^{-4}.

opacities and ^{12}CO emission at any velocity. The concentration of ^{12}CO emission on the western end of Cas A at velocities between −35.5 and −40 km s^{-1} is not seen in the C270α opacities. ^{12}CO emission in the velocity range −45.2 to −47.8 km s^{-1} shows a gradient from northwest to southeast, whereas the gradient in the C270α opacities is from northeast to southwest. While there is significant C270α opacity at velocities of −49.4 and −50.8 km s^{-1}, there is practically no ^{12}CO emission at these velocities. Similar conclusions are reached by comparing the C270α opacity distribution (Fig. 3) with that of H_2O observed by de Jager et al. (1978) with an angular resolution of 2.″6. The λ2 cm H_2CO observations of Batrla, Wilson, & Martin-Pintado (1983) with a resolution of 1′ show that the −37 km s^{-1} feature is concentrated only near the western edge of Cas A, whereas the −47 km s^{-1} feature is concentrated near the southeastern edge. No absorption is seen in other parts of Cas A. The C270α line, on the other hand is seen over most parts of Cas A at both velocities. Higher angular resolution observations of H_2CO (with 10″ by Goss et al. 1984) and OH (with 7″ by Bieging & Crutcher 1986) reveal that the molecular clouds are mostly concentrated toward the southern half of Cas A. On the other hand, high-resolution H I observations (Bieging et al. 1991) show that there is H I over the entire face of Cas A. With our angular resolution we see that the C270α is present over the entire face of Cas A, which is more like H I than molecular gas.

In order to improve the S/N of the C270α maps, and therefore to get a better comparison, we averaged the opacity maps for each of the three features over their respective velocity ranges. Similar average opacity maps for H I and average emis-

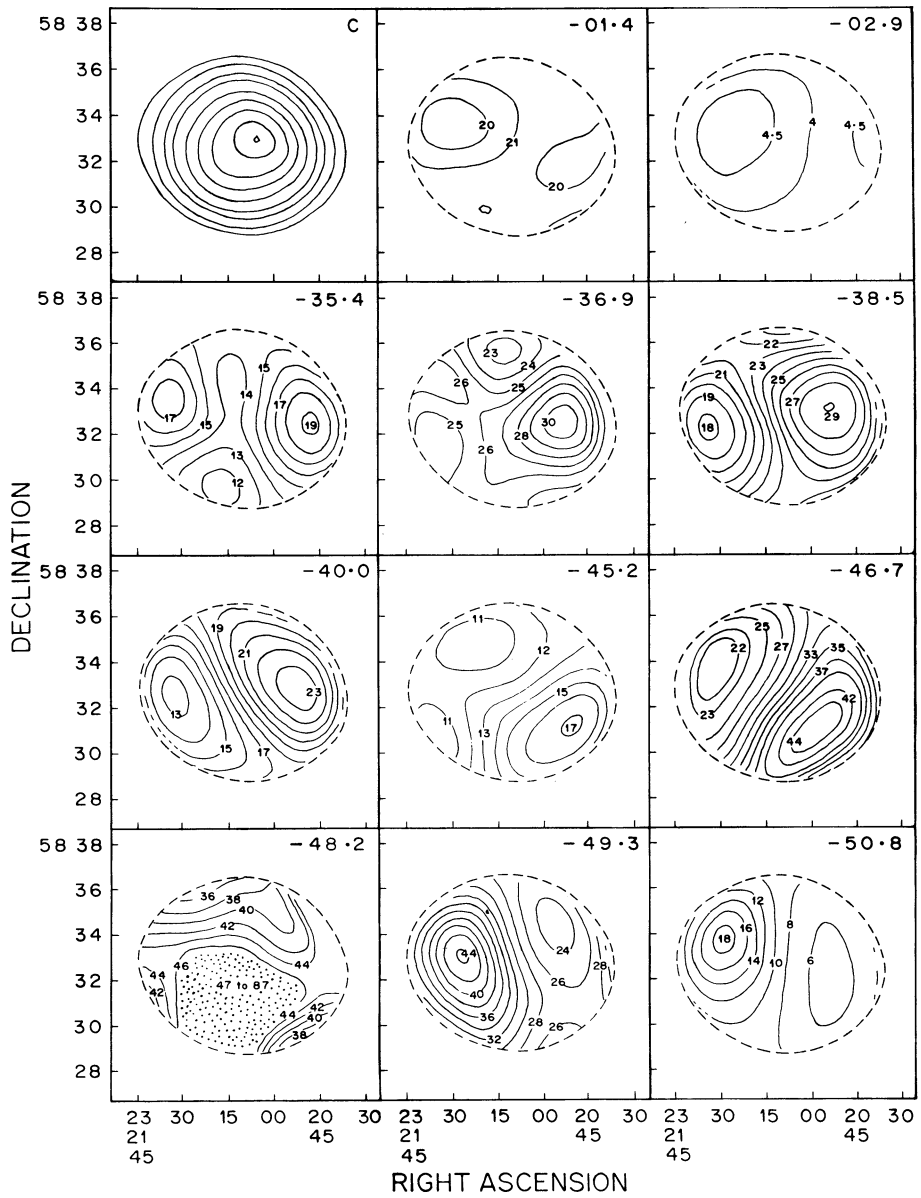

FIG. 4.—The distribution of H I optical depths obtained with the same angular resolution as in Fig. 3. The velocity resolution is 1.55 km s^{-1} and the central velocity for each image is indicated at the top right corner. The image at the top left corner, marked C, is the continuum image of Cas A at $\lambda = 21$ cm. Contour levels for this image are 3, 4, 6, 8, 12, 16, 20, 24, 26 units where 1 unit = 100 Jy beam.$^{-1}$ Contour levels for the optical depth images are as marked with 1 unit = 0.1. The optical depth image at -48.2 km s^{-1} is saturated in the dotted region.

sion maps for ^{12}CO were computed. The data at -48 km s^{-1}, where the H I is saturated, are left out in all three cases. For this feature, two separate averages were computed from the unsaturated wings of the profile. The results are shown in Figure 6. The C270α and H I distributions centered at -37, -46, and -50 km s^{-1} are remarkably similar, although not identical. At -37 km s^{-1} there is a concentration of both H I and C270α is the western half of the source and a low optical depth region in the southeast corner. At -46 km s^{-1} the high optical depth region is toward the southwest corner in both maps. The gradients are also in the same direction. At -50 km s^{-1} there is a concentration toward the northeast region in both H I and C270α opacities. At this velocity the C270α opacity shows some structure in the western half of the source, where the H I opacity is low but essentially smooth. The opacity distributions of the Orion arm feature centered at -2 km s^{-1} do not show similarities to the same degree, although the higher opacity in the western half seen in H I is also reflected in the C270α optical depth. No similarity is seen in the C270α and ^{12}CO distributions shown in Figure 6.

In conclusion, there is good agreement between the H I and C270α opacity distributions across the face of Cas A and very little similarity between C270α and molecular line distributions. The H I and C270α distributions are, however, not identical. Bieging et al. (1991) have shown that high angular and velocity resolution reveals an abundance of fine structure in the H I opacity distribution. With small changes in velocity, the distribution of H I optical depths changes dramatically. There-

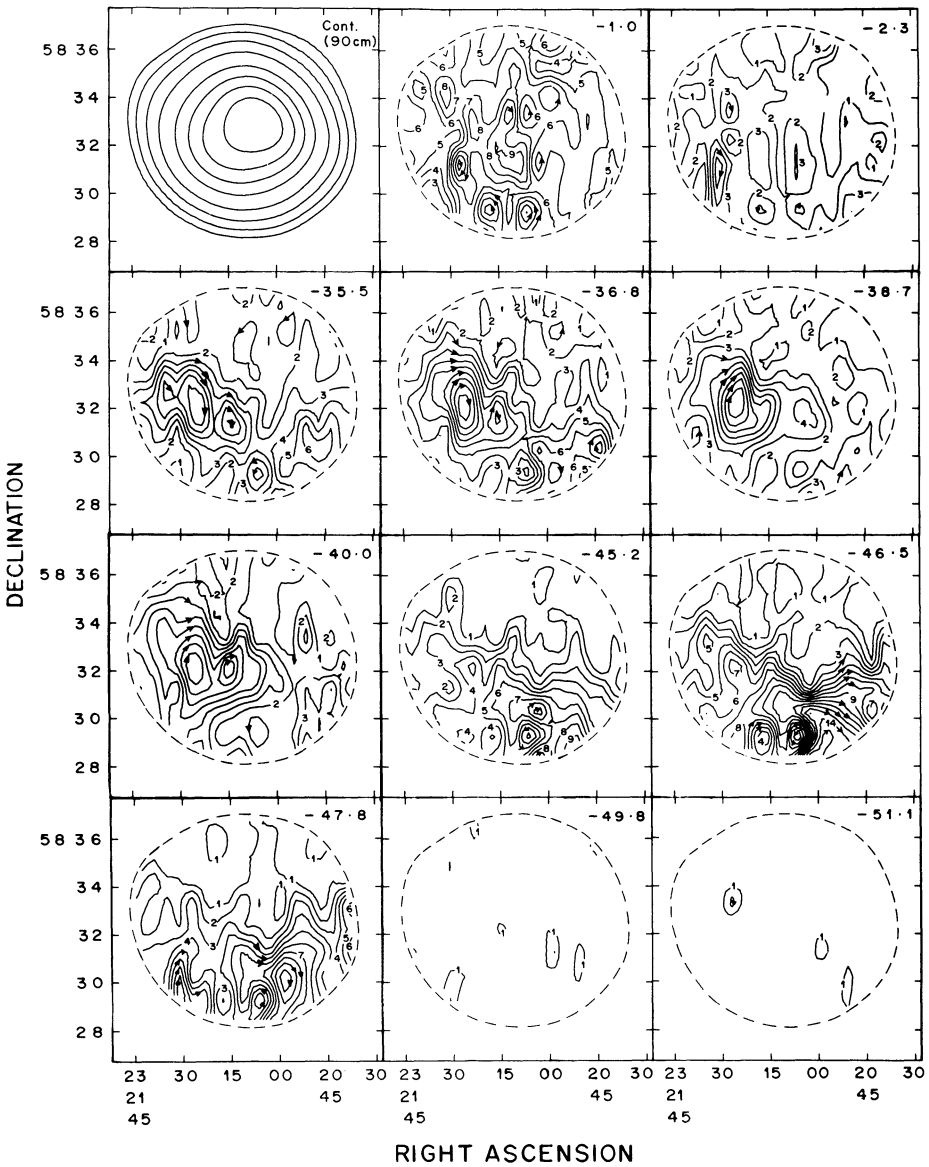

FIG. 5.—Distribution of ^{12}CO emission over the face of Cas A near the velocities where C270α recombination line is observed (see Fig. 3). The beam size is ~1′ and the velocity resolution is 1.3 km s^{-1}. The top left image shows the continuum emission at 332 MHz with same contour levels as in Fig. 2. Contour levels for the ^{12}CO emission are as marked with 1 unit = 0.3 K of antenna temperature corrected for atmospheric absorption (T_A^*). Contours with clockwise arrows show increasing levels.

fore, some of the differences between H I and C270α could be due to the differences in the central velocity and resolution of the two distributions.

4. DISCUSSION

In this paper we have presented VLA observations of the C270α line emission toward Cas A and compared our maps to H I and molecular line maps of similar resolution. These observations favor the association of C270α emission with regions of neutral atomic hydrogen rather than molecular clouds. The correspondence between C270α and H I is not one-to-one, and some of the differences could be attributed to the difference in the central velocities and angular resolutions of the two observations. Higher angular resolution C270α observations will help clarify this.

The association of C270α region with the H I clouds is reasonable from the point of view of the geometry of the clouds as well. Although the C270α optical depth images presented here (Fig. 3) show some structure, the overall distribution suggests that the clouds, taken together, cover the entire face of Cas A. This implies that the lateral extent of the emission region is a few parsecs. As discussed in a second paper (PAE94), combining the electron density and emission measure derived from model fitting gives a path length through the emission region, and the best-fitting model has a path length of a few parsecs—comparable to the lateral extent of the emitting gas. On the other hand, if the temperature is of the order 20 K (as it would be if C270α regions are associated with molecular clouds), then the path length through the line region would be a few hundredths of a parsec, implying an unlikely face-on sheet geometry for the gas.

The identification of the C II region toward Cas A with H I

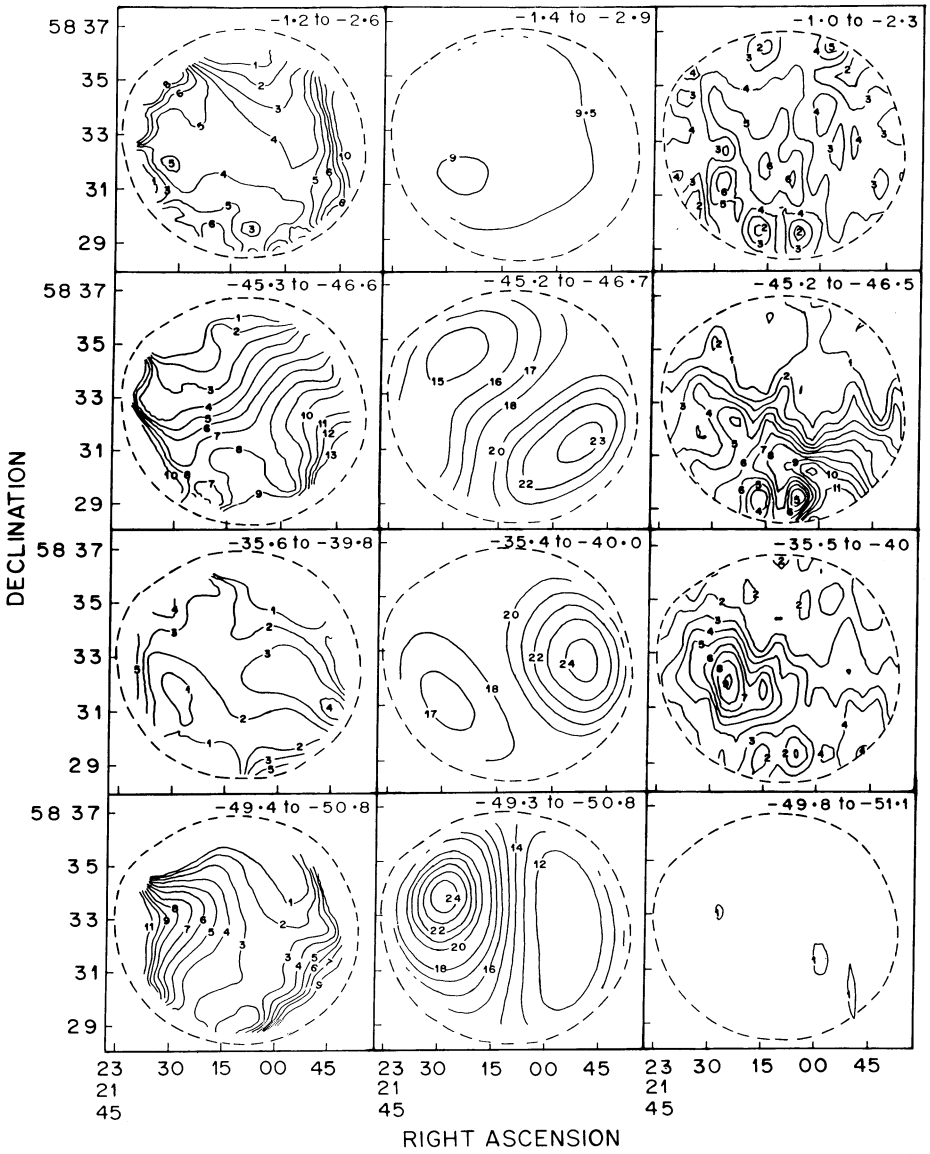

FIG. 6.—Comparison of the distribution of C270α (*left column*) and H I optical depths (*middle column*) and ^{12}CO emission (*right column*) over the face of Cas A in four velocity ranges which are indicated in each frame. First row correspond to the Orion arm and the third row to the Perseus arm at -37 km s^{-1}. The second and fourth rows correspond to the wings of the Perseus arm feature at -47 km s^{-1}. Contour levels are as marked with 1 unit = 2×10^{-4} for C270α, 0.1 for H I, and 0.3 K for ^{12}CO maps.

clouds in the same direction has the advantage that it is possible to combine the results of recombination lines and λ21 cm H I measurements to learn more about physical conditions in the cloud. The challenge, then, would be to find a sensible set of physical conditions that explain the complete set of recombination line observations of Cas A and the λ21 cm H I observations. This challenge is taken up in a second paper (PAE94), where we conclude that the only model with physical conditions that make sense is one in which the recombination lines and λ21 cm H I absorption both arise from atomic gas with a temperature near 35 K.

The VLA is a part of the National Radio Astronomy Observatory which is operated by the Associated Universities, Inc., under a cooperative agreement with the NSF. K. R. A. thanks the Space Telescope Science Institute of hospitality during part of this work.

REFERENCES

Baars, J. M. W., Genzel, R., Pauliny-Toth, I. I. K., & Witzel, A. 1977, A&A, 61, 99
Batrla, W., Walmsley, C. M., & Wilson, T. L. 1984, A&A, 136, 127
Batrla, W., Wilson, T. L., & Martin-Pintado, J. 1983, A&A, 119, 139
Bieging, J. H., & Crutcher, R. M. 1986, ApJ, 310, 853
Bieging, J. H., Goss, W. M., & Wilcots, E. M. 1991, ApJS, 75, 999
Blake, D. H., Crutcher, R. M., & Watson, W. D. 1980, Nature, 287, 707
de Jager, G., Graham, D. A., Wielebinski, R., Booth, R. S., & Gruber, G. M. 1978, A&A, 64, 17
Ershov, A. A., Ilyasov, Yu. P., Lekht, E. E., Smirnov, G. T., Solodkov, V. T., & Sorochenko, R. L. 1984, Soviet Astron. Lett., 10, 348
Ershov, A. A., Lekht, E. E., Smirnov, G. T., & Sorochenko, R. L. 1987, Soviet Astron. Lett., 13, 8
Goss, W. M., Kalberla, P. M. W., & Dickel, H. R. 1984, A&A, 139, 317

Kalberla, P. M. W., Schwarz, U. J., & Goss, W. M. 1994, to be published
Konovalenko, A. A. 1990, in Radio Recombination Lines: 25 Years of Investigation, ed. M. A. Gordon & R. L. Sorochenko (Dordrecht: Reidel), 209
Payne, H. E., Anantharamaiah, K. R., & Erickson, W. C. 1989, ApJ, 341, 890 (PAE89)
———. 1994, ApJ, 430, 690 (PAE94)
Salem, M., & Brocklehurst, M. 1979, ApJS, 39, 633
Schwarz, U. J., Troland, T. H., Albinson, J. S., Bregman, J. D., Goss, W. M., & Heiles, C. E. 1986, ApJ, 301, 320
Shaver, P. A. 1975, Pramana, 5, 1
Sorochenko, R. L., & Smirnov, G. T. 1990, in Radio Recombination Lines: 25 Years of Investigation, ed. M. A. Gordon & R. L. Sorochenko (Dordrecht: Reidel), 189
Sorochenko, R. L., & Walmsley, C. M. 1991, A&A, Trans., 1, 31
Troland, T. H., Crutcher, R. M., & Heiles, C. E. 1985, ApJ, 298, 808
Walmsley, C. M., & Watson, W. D. 1982, ApJ, 260, 317
Watson, W. D., Western, L. R., & Christensen, R. B. 1980, ApJ, 240, 956